ROYAL SOCIETY
OF CHEMISTRY

PAPER

Check for updates

Blocking tau transmission by biomimetic graphene nanoparticles†

Runyao Zhu, [ID] [a] Kamlesh M. Makwana, [ID] [b] Youwen Zhang,[a] Benjamin H. Rajewski, [ID] [b] Juan R. Del Valle [ID] *[b] and Yichun Wang [ID] *[a]

Tauopathies are a class of neurodegenerative diseases resulting in cognitive dysfunction, executive dysfunction, and motor disturbance. The primary pathological feature of tauopathies is the presence of neurofibrillary tangles in the brain composed of tau protein aggregates. Moreover, tau aggregates can spread from neuron to neuron and lead to the propagation of tau pathology. Although numerous small molecules are known to inhibit tau aggregation and block tau cell-to-cell transmission, it is still challenging to use them for therapeutic applications due to poor specificity and low blood-brain barrier (BBB) penetration. Graphene nanoparticles were previously demonstrated to penetrate the BBB and are amenable to functionalization for targeted delivery. Moreover, these nanoscale biomimetic particles can self-assemble or assemble with various biomolecules including proteins. In this paper, we show that graphene quantum dots (GQDs), as graphene nanoparticles, block the seeding activity of tau fibrils by inhibiting the fibrillization of monomeric tau and triggering the disaggregation of tau filaments. This behavior is attributed to electrostatic and π–π stacking interactions of GQDs with tau. Overall, our studies indicate that GQDs with biomimetic properties can efficiently inhibit and disassemble pathological tau aggregates, and thus block tau transmission, which supports their future developments as a potential treatment for tauopathies.

Introduction

Pathogenic aggregation of tau proteins into neurofibrillary tangles (NFTs) is a characteristic feature of tauopathies, which are a group of neurodegenerative diseases, including Alzheimer's disease (AD),[1] frontotemporal dementias (FTDP-17),[2] Pick's disease,[3] and progressive supranuclear palsy.[4] The normal function of tau is to stabilize microtubules by binding with tubulin in neurons. These microtubules provide a structural backbone for axons and dendrites and serve as 'railways' for the transport of proteins and organelles in axons and dendrites.[5] Pathogenic fibrillization of tau reduces cytoskeletal stability, interferes with synaptic transmission and axonal transport, and causes aberrant communication between neurons.[6] These insoluble tau deposits can arise due to gene mutations or aberrant post-translational modifications such as hyperphosphorylation and acetylation.[2,7,8] In addition, tau aggregates can spread from neuron to neuron and induce the misfolding of normal soluble tau, leading to the

propagation of tau pathology in a prion-like manner.[9,10] Small molecule library screening campaigns have identified several compounds that either directly or indirectly inhibit tau aggregation.[11,12] These molecules include modulators of tau post-translational modification,[8] microtubule stabilizers,[13] tau assembly inhibitors,[13,14] and degradation promoters.[15] However, there are no disease-modifying drugs that target tau aggregation. Moreover, many drug candidates suffer from limited penetration of the blood-brain barrier (BBB) and off-target effects, reducing central nervous system bioavailability and limiting their clinical utility.[15,16] Furthermore, compounds targeting kinases upstream of tau may disrupt other physiological processes resulting in undesirable side effects such as an increased risk of diabetes and arrhythmia.[17] Therefore, developing novel strategies to overcome current challenges is critical for the treatment of neurodegenerative tauopathies.

Nanoparticles (NPs), as nanocarriers, have demonstrated the ability to deliver drugs into the brain and are capable of controlled release and targeted delivery.[18,19] Graphene quantum dots (GQDs), as graphene-based NPs, are single or a-few layered graphene with lateral dimensions typically less than 20 nm.[20] These nanosheets have garnered much attention in biomedicine, including bioimaging, biosensor, and cancer phototherapy, due to their unique optical, electrochemical, and physicochemical properties, high biocompatibility, and low cytotoxicity.[21–24]

[a] Department of Chemical & Biomolecular Engineering, University of Notre Dame, Indiana 46556, USA. E-mail: ywang65@nd.edu

[b] Department of Chemistry & Biochemistry, University of Notre Dame, Indiana 46556, USA

† Electronic supplementary information (ESI) available. See DOI: **https://doi.org/10.1039/d3tb00850a**

Moreover, GQDs can be used as nanocarriers in drug delivery systems upon conjugation with target ligands and chemotherapeutic agents *via* either covalent or noncovalent bonds because of their surface functional groups and π-conjugated planar structure.[25] GQD-based drug delivery systems[26–28] were previously demonstrated to penetrate the BBB and specifically target brain tumor regions, suggesting great potential in neuroscience therapeutics. Most importantly, GQDs exhibit a wide spectrum of biomimetic properties, including polarizability, amphiphilic character, and participation in electrostatic interactions, hydrophobic interactions, hydrogen bonding, and π–π stacking.[29,30] Thus, GQDs can self-assemble[31] or assemble with various proteins, such as amyloid-β (Aβ) peptides,[32,33] biofilm amyloids,[34] and α-synuclein,[28] demonstrating their potential to protect against the neuronal damage associated with AD and Parkinson's disease. Furthermore, the properties of GQDs, such as size,[35] charge,[36] functional groups,[37] and chirality,[38] can be engineered precisely, affording opportunities to modulate their assembly with proteins.[39,40]

Here, we report that biomimetic GQDs are able to block the seeding activity of tau fibrils in an *in vitro* cellular tau biosensor propagation model. To investigate the effect of GQDs on tau propagation, we engineered GQDs with different sizes and charges by post-separation technologies and functionalization of GQDs with cysteine (Cys) and ethylenediamine (EDA) and studied the interaction between tau and GQDs *in vitro*. By monitoring the amount of tau aggregates, the secondary structure, and the morphology of tau, we found that negatively charged GQDs with a larger size inhibited tau aggregation more effectively. In addition, the presence of GQDs induced the disaggregation of tau filaments *in vitro*. These findings were potentially attributed to the fact that aromatic residues on the

aggregation-prone region of tau can interact with GQDs *via* π–π stacking interactions, as verified by the fluorescence quenching assay. The positively charged microtubule-binding domain of tau can interact with carboxyl groups on the edge of GQDs *via* electrostatic interactions. Furthermore, a cellular propagation assay employed to test the seeding activity of tau fibrils demonstrated that GQDs blocked the aggregation of endogenous tau induced by extracellular seeds. Overall, our findings suggest that engineered biomimetic GQDs are a promising and effective platform to prevent the cellular transmission of tau by inhibition and disassembly of tau aggregates.

Results and discussion

As-synthesized GQDs carrying carboxyl groups on the edges in an average diameter of 8 nm were obtained by the previously reported method (Fig. 1a–c, Fig. S1 and S2a, ESI†). The heights of as-synthesized GQDs are between 0.5 and 2 nm, corresponding to 1–3 graphene layers (Fig. S2b, ESI†).[35] The zeta potential of as-synthesized GQDs was -19.9 ± 2.30 mV (Fig. 1d and Fig. S4, ESI†). To obtain GQDs with different charges, we reduced the negative charge by conjugating as-synthesized GQDs with cysteine (Cys) and ethylenediamine (EDA) *via* carboxyl groups (Fig. 1a and Fig. S1 and S3, ESI†). In the Fourier transform infrared (FTIR) spectra (Fig. 1c), due to the carboxyl groups in the structure of Cys, the peak at 1706 cm^{-1} assigned to C=O stretching was more obvious in the spectrum of Cys-GQDs than those of as-synthesized GQDs and EDA-GQDs.[35] The FTIR spectra of Cys-GQDs and EDA-GQDs also appeared peaks at 1250 and 1184 cm^{-1} attributed to C–N stretching.[19] The zeta potentials of Cys-GQDs and EDA-GQDs were -1.46 ± 0.42 mV
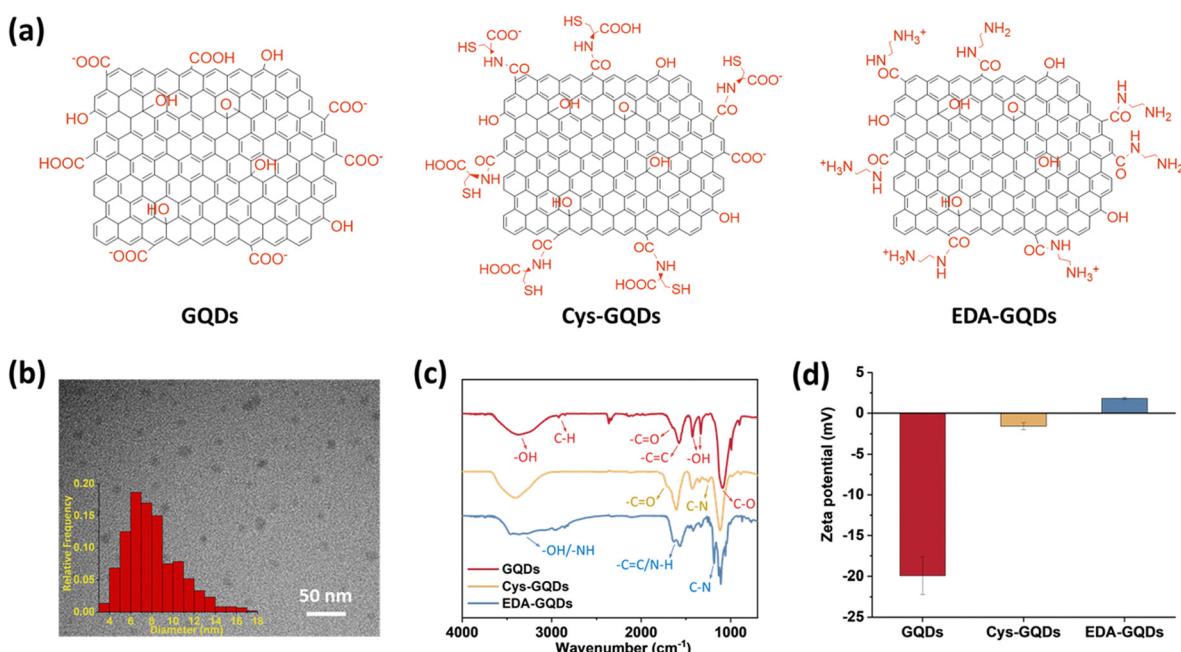

Fig. 1 (a) Molecular structure, (b) transmission electron microscope (TEM) image and size distribution of GQDs. The average diameter is 8.1 ± 2.5 nm. (Scale bar: 50 nm.) (c) Fourier transform infrared (FTIR) spectra and (d) zeta potentials of GQDs, Cys-GQDs, and EDA-GQDs.

and 1.63 ± 0.55 mV (Fig. 1d and Fig. S4, ESI†), due to the pKa value of Cys and EDA, 1.71 and 10.7, respectively.

Following the synthesis, characterization, and functionalization of GQDs, we investigated the charge effect of GQDs on the aggregation of a recombinant 0N4R isoform of tau. Tau used in these studies includes a P301L mutation (tau_{P301L}) which is frequently observed in patients with FTDP-17 (Fig. S5, ESI†).[41] This missense mutation leads to a two-fold increase in aggregation rate compared with the full-length tau.[42] Tau_{P301L} contains four microtubule-binding repeat domains (R1–R4) that harbor two key aggregation-prone motifs: PHF6* (VQIINK, residues

217–222) and PHF6 (VQIVYK, residues 248–253).[7] A large number of basic residues result in an overall positive charge in the repeat domains at physiological pH (Fig. 2a). Firstly, the aggregation of tau_{P301L} was monitored by a ThT fluorescence assay (Fig. 2b). ThT is a benzothiazole dye that exhibits enhanced fluorescence upon binding to tau fibers with β-sheet secondary structure.[43] In the presence of heparin sulfate, tau_{P301L} was induced to aggregate, resulting in a sigmoidal curve from increased ThT fluorescence (Fig. 2c). Incubation of tau_{P301L} in the presence of heparin and 6.25 μM GQDs or Cys-GQDs resulted in 99% inhibition of endpoint ThT fluorescence
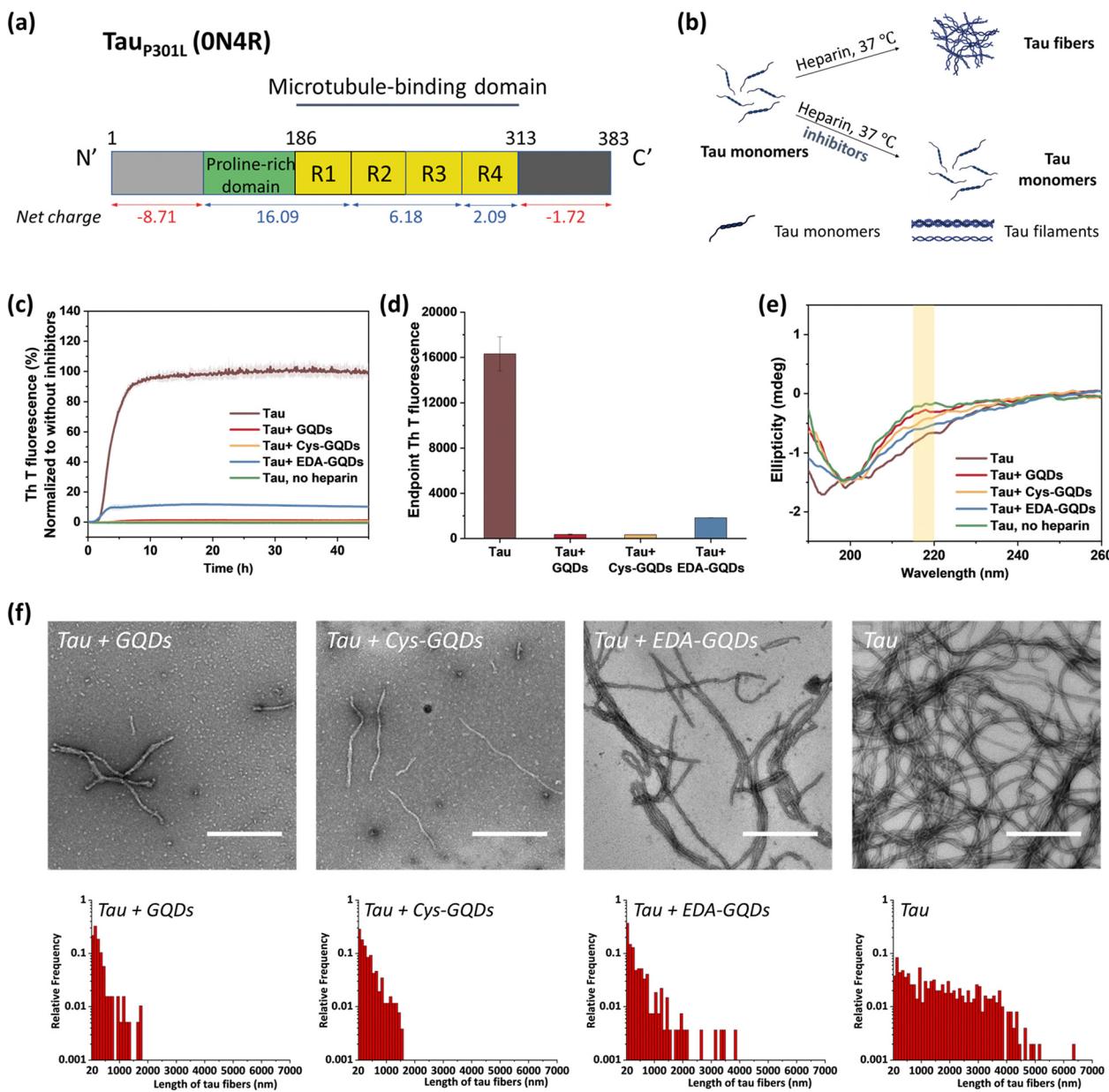
Fig. 2 Tau_{P301L} aggregation was inhibited by GQDs, Cys-GQDs, and EDA-GQDs. (a) Aggregation-prone tau_{P301L} sequence. (b) Schematic representation of the *in vitro* aggregation of recombinant tau (10 μM) in the presence and absence of inhibitors at a concentration of 6.25 μM. (c) and (d) In the presence of GQDs or functionalized GQDs, thioflavin T (ThT) fluorescence of tau aggregation was reduced significantly. The inhibitory effect of EDA-GQDs is weaker than GQDs and Cys-GQDs. (e) Circular dichroism (CD) spectra, (f) TEM images, and length distributions of tau protein incubated with/without 6.25 μM GQDs or functionalized GQDs for 4 days. (Scale bars: 500 nm)

7380 | *J. Mater. Chem. B*, 2023, **11**, 7378–7388

This journal is © The Royal Society of Chemistry 2023

(Fig. 2c and d). However, EDA-GQDs with overall positive charge exhibited 88.8% inhibitory activity, less effective than the negatively charged GQDs and Cys-GQDs.

The mechanism of tau aggregation in the presence of heparin is widely described as ligand-induced nucleation-dependent polymerization (NDP).[44] The lag time (t_{lag}) and the apparent elongation rate constant (k_{app}) of the aggregation process were derived by fitting each kinetic data to a Gompertz growth function (Table S1, ESI†).[45,46] The lag time represents the time of nucleation process (*i.e.*, initial seed formation of tau) and the apparent elongation rate constant represents the rate of growth process (*i.e.*, the elongation of tau fibrils). The tau aggregation without GQDs as a control showed a t_{lag} of 1.84 ± 0.01 h and a k_{app} of 0.76 ± 0.008 h^{-1}. In the presence of GQDs or Cys-GQDs, t_{lag} was increased to nearly double that of the control sample, while k_{app} was reduced to 0.70 ± 0.039 and 0.38 ± 0.021 h^{-1}, a decrease of 7.9% and 50% compared to the control sample, respectively. These results suggest that GQDs and Cys-GQDs impeded both seed formation and the fibril elongation processes. In contrast, tau incubated with EDA-GQDs led to a significant decrease in t_{lag}, potentially because the presence of EDA-GQDs increased the local concentration of soluble monomeric tau, facilitating the formation of aggregation-prone tau seeds. Despite a decreased t_{lag}, k_{app} was slightly increased, possibly because a portion of the aggregation-inducer polyanion heparin interacted with EDA-GQDs with positive charge, reducing the formation of tau fibers by 88.8% after 45 h incubation compared to the control sample.

We detected the effect of GQDs and functionalized GQDs on the secondary structure transition of tau$_{P301L}$ using circular dichroism (CD) spectroscopy (Fig. 2e). In the absence of heparin, soluble tau monomers showed a negative peak at $\sim$200 nm, indicative of a random coil conformation. After heparin-induced fibrillization, a growing CD signal at $\sim$218 nm, typical of β-sheet conformation, emerged.[47] Upon incubation with GQDs, Cys-GQDs, or EDA-GQDs for 4 days, the CD intensity of tau at 218 nm was reduced by 61%, 39%, and 18% compared to the control sample, respectively, suggesting inhibition of transition to a β-rich tau assembly. The secondary structure of tau had less β-sheet content in the presence of GQDs or Cys-GQDs than in the presence of EDA-GQDs, which is consistent with the ThT assay results (Fig. 2c).

The morphological features of tau$_{P301L}$ fibrils were examined using transmission electron microscopy (TEM) after incubation for 4 days. To quantify the tau fibers in each sample, we measured their length and density using ImageJ (Fig. 2f and Table S2, ESI†). The aggregation of tau in the control sample resulted in the formation of filaments with an average length of 1623 ± 1255 µm and an average density of 4.53 ± 2.08 fibers per µm^2. In the presence of GQDs or functionalized GQDs, heparin-induced tau$_{P301L}$ assembled into shorter fibers with lower density. When tau$_{P301L}$ monomers were incubated with GQDs, Cys-GQDs, or EDA-GQDs, the average length of formed fibers was decreased to 17%, 20%, and 35% of the control sample, while the average density of fibers was decreased to 30%, 34%, and 78%, compared to that of the control sample. Among samples incubated with the three GQDs, tau incubated with EDA-GQDs resulted in the formation of 3 to 4-fold more fibers per unit area than tau with GQDs or Cys-GQDs. The collective results indicate that GQDs and Cys-GQDs with negative charges have a better inhibitory effect on the fibrillization of tau than EDA-GQDs with positive charge.

To further investigate whether the degree of negative charge on GQDs can influence their inhibitory efficiency, we monitored the ThT fluorescence of tau$_{P301L}$ incubated with GQDs or Cys-GQDs at different concentrations. GQDs and Cys-GQDs inhibited aggregation in a dose-dependent manner (Fig. 3a). We obtained IC$_{50}$ value for GQDs and Cys-GQDs by fitting the dose-response results to a sigmoidal function (Fig. 3b). The IC$_{50}$ of GQDs and Cys-GQDs are 0.70 µM, and 0.89 µM.[12,14] These results suggest that when the zeta potential of GQDs is between -20 mV and -1.5 mV, the amount of negative charges on GQDs does not affect the inhibitory efficiency significantly.

Before investigating the effect of GQDs on tau propagation in the cellular assay, we determined the cytotoxicity of GQDs, Cys-GQDs, and EDA-GQDs by employing the CCK-8 assay with SH-SY5Y human neuroblastoma cells. GQDs and Cys-GQDs exhibited no appreciable toxicity toward SH-SY5Y cells up to 5 µM, whereas 5 µM of EDA-GQDs reduced cell viability by 90.7% after 48 h incubation (Fig. S6, ESI†). It is likely that positively charged EDA-GQDs interact with the negatively charged cell membrane, resulting in higher cell uptake and disruption of membrane integrity.[48] Therefore, we only
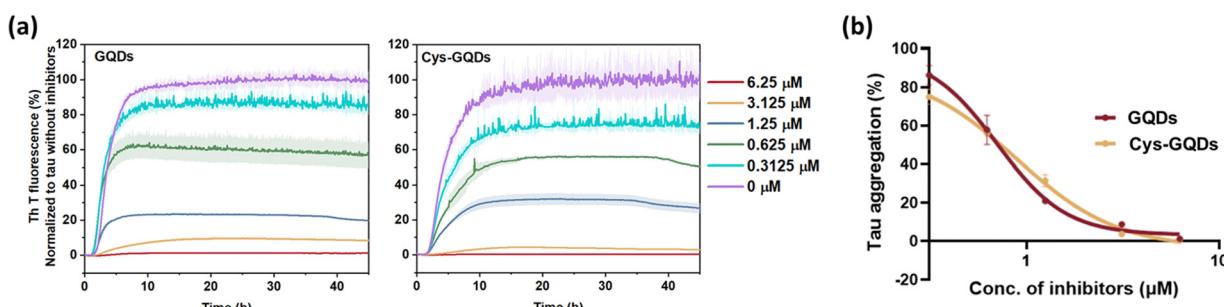
Fig. 3 (a) ThT fluorescence of tau aggregation was decreased with the increased concentration of GQDs and Cys-GQDs. (b) Dose–response results of ThT fluorescence assay of GQDs and Cys-GQDs were fitted to a sigmoidal model. The IC$_{50}$ of GQDs and Cys-GQDs is 0.70 µM and 0.89 µM, respectively, obtained from the dose–response curve.
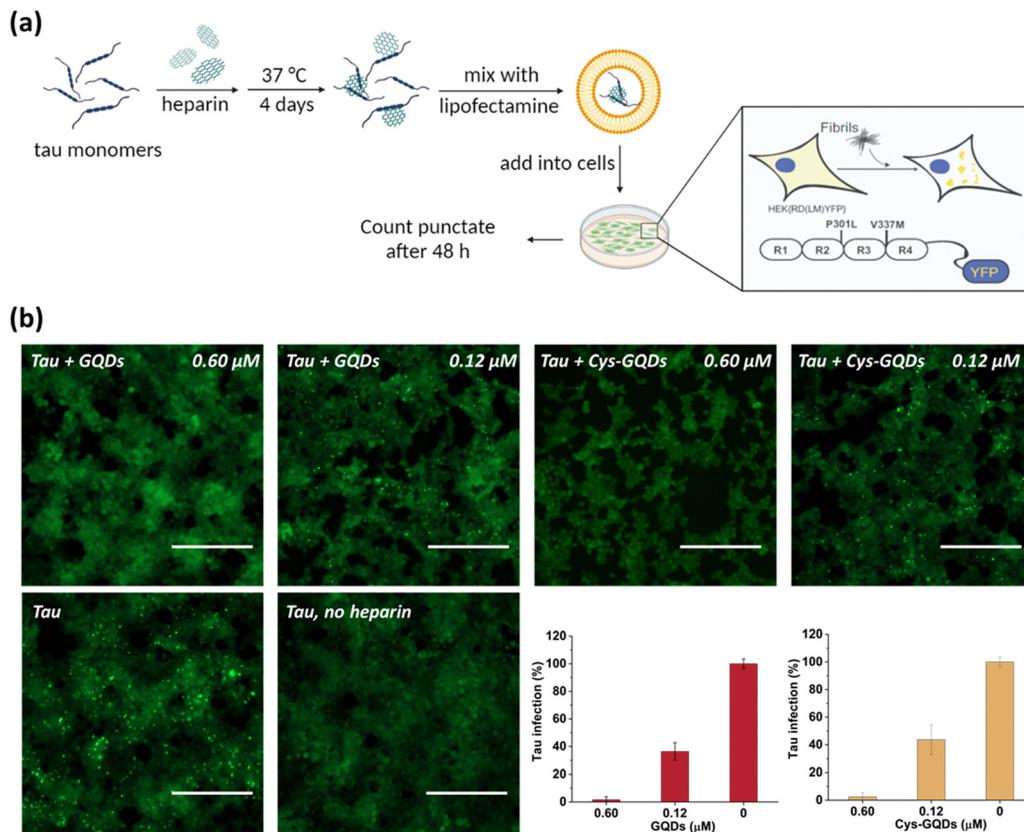
Fig. 4 (a) Scheme of HEK293 cellular tau biosensor propagation assay. (b) GQDs and Cys-GQDs prevented the cellular seeding of tau$_{P301L}$ monomers. Soluble monomeric tau$_{P301L}$ (0.19 μM) in the presence of heparin was incubated with GQDs or Cys-GQDs for 4 days and then added to HEK293 cells stably expressing tau-RD (P301L/V337M)–YFP. Representative images of cells were taken at 20× magnification under fluorescein isothiocyanate (FITC) channel (ex: 469 nm/em: 525 nm). The green puncta with high fluorescence represented the aggregation of tau in cells induced by exogenous tau fibers. Scale bar: 200 μm. Bar graphs show the number of intracellular fluorescent puncta relative to control infection wells without inhibitors.

considered the nontoxic GQDs and Cys-GQDs in the following cellular assay.

One of the key characteristics of tau NFTs is cellular transmission from one diseased neuron to adjacent healthy neurons, inducing the propagation of tau pathology.[9,10] To examine whether GQDs and Cys-GQDs can inhibit the cellular seeding of recombinant tau, we employed HEK293 biosensor cells that stably expressed a tau-yellow fluorescent protein fusion [tau-RD(LM)-YFP] (Fig. 4a).[49] After incubating preformed tau$_{P301L}$ fibrils with these cells for 48 h, the aggregation of endogenous tau induced by extracellular seeds can be monitored by detection of focal puncta with green fluorescence. The quantitative measurements of intracellular aggregates were provided by automated image analysis of green puncta. Monomeric tau has no capacity to seed the aggregation of endogenous tau and the cells remain diffusely fluorescent with no focal puncta. Pre-treatment of tau$_{P301L}$ monomers with 0.12 μM of GQDs or Cys-GQDs in the presence of heparin decreased the intracellular aggregates by 60% relative to the control treatment. As concentrations of GQDs and Cys-GQDs increased, the seeding activity of tau$_{P301L}$ decreased. With 0.6 μM of GQDs or Cys-GQDs, the seeding activity of tau$_{P301L}$ was almost completely abolished (Fig. 4b). These results demonstrate that GQDs and Cys-GQDs

prevent the fibrillization of tau monomers and thus block the cellular seeding activity of recombinant tau.

The presence of NFTs in the brain, which are composed of tau aggerates, is the primary feature of tauopathies. Promoting the disaggregation of tau fibrils is thus considered a potential strategy for therapeutic development.[15] We investigated the effect of GQDs on the disaggregation of mature tau fibrils using the ThT fluorescence assay (Fig. 5a). After incubation with GQDs, Cys-GQDs, or EDA-GQDs, the intensity of ThT fluorescence in the presence of tau fibrils decreased with time (Fig. 5b), suggesting that tau fibrils could be dissociated into tau monomers and oligomers. Based on endpoint ThT fluorescence after 30 h (Fig. 5c), GQDs, Cys-GQDs, and EDA-GQDs induced 56%, 81%, and 92% disassembly of tau fibrils. TEM images of tau fibrils treated with GQDs and engineered GQDs also revealed the disaggregation of tau filaments into fibril fragments (Fig. S7, ESI†). To quantify the tau NFTs after the disassembly by GQDs, we measured the area of tau NFTs in each sample using ImageJ (Table S3, ESI†). In the presence of GQDs, Cys-GQDs, or EDA-GQDs, tau NFTs were 33%, 89%, and 52% disassembled. This is potentially due to the negatively charged fuzzy coat of tau$_{P301L}$ fibrils comprised of the unfolded C-terminal and N-terminal domains (Fig. 2a) that surrounds

7382 | *J. Mater. Chem. B*, 2023, **11**, 7378–7388

This journal is © The Royal Society of Chemistry 2023
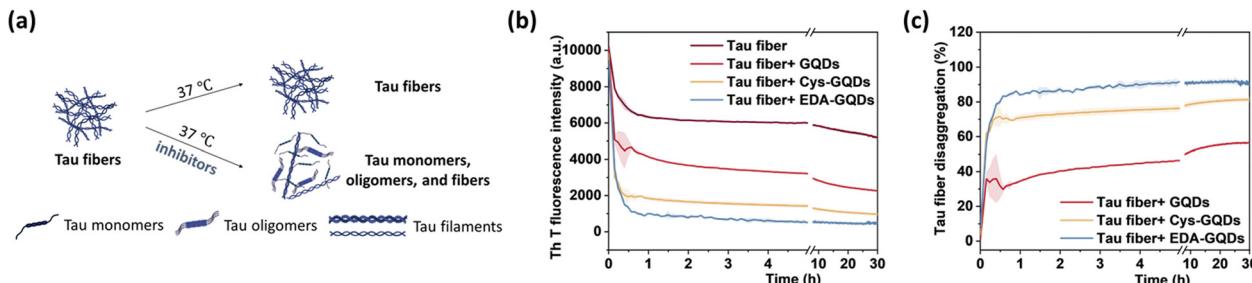
Fig. 5 (a) Scheme of the *in vitro* disaggregation assay of tau fibers (5 μM) in the presence and absence of inhibitors (6.25 μM). (b) ThT fluorescence of tau fibers and (c) the percentage of disaggregation of preformed tau fibers after incubation with GQDs, Cys-GQDs, or EDA-GQDs.

the fibrillar tau core.[50] The negative charges on the outermost layer of tau fibers could prevent GQDs from approaching, whereas Cys-GQDs and EDA-GQDs with fewer charges could pass through the fuzzy coat and reach the fibrillar tau core more easily. In addition, negatively charged Cys-GQDs are more likely to interact with the positively charged fibrillar core and disaggregate the tau fibrils, compared to EDA-GQDs with positive charge. In the ThT fluorescence assay, the presence of EDA-GQDs could affect ThT binding with tau fibers due to their positive charge, and thus ThT fluorescence of tau fibrils treated by EDA-GQDs was reduced much more than the actual fiber disassembly obtained from TEM images. Due to the toxicity of some types of soluble tau dimer, trimer, and oligomers on neurons,[51] we tested the cytotoxicity of tau NFTs after disaggregation by GQDs and engineered GQDs on SH-SY5Y cells. The disaggregated fibrils did not exhibit cytotoxicity toward SH-SY5Y cells after 48 h incubation (Fig. S8, ESI†).

To further investigate the effect of GQDs and Cys-GQDs on tau propagation, we tested if they can block the cellular transmission of mature tau fibrils in the tau biosensor seeding assay. After 36 h treatment of GQDs or Cys-GQDs with pre-formed tau fibrils, HEK293 cells expressing tau-RD(LM)-YFP were incubated with the pre-treated tau fibrils. With the increase in concentration from 0.12 μM to 0.5 μM, GQDs reduced the aggregation of endogenous tau from 18% to 80%, while Cys-GQDs reduced the intracellular aggregates from 6% to 88% compared to the control sample without GQDs or Cys-GQDs (Fig. 6). To confirm whether GQDs or Cys-GQDs simply affect lipofectamine-mediated cellular uptake of tau fibrils rather than the seeding capacity of the fibrils themselves, we mixed tau fibrils with GQDs or Cys-GQDs without incubation and then incubated the mixture with cells for 48 h. GQDs and Cys-GQDs did not reduce the aggregation of endogenous tau without prior incubation, suggesting that GQDs and Cys-GQDs did not interfere with lipofectamine-mediated cellular uptake of tau fibrils (Fig. S9, ESI†) and the decrease of intracellular aggregates was solely attributed to fibril disassembly into seed incompetent monomers after 36 h incubation with GQDs or Cys-GQDs, effectively blocking the seeding capacity of mature tau fibrils.

Based on our experimental results, negatively charged GQDs can inhibit the fibrillization of tau proteins more efficiently than GQDs with positive charge. This suggests that the positively
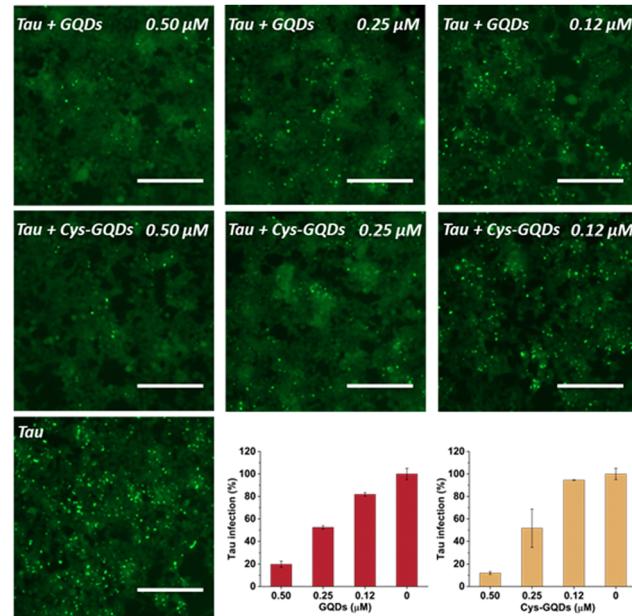

Fig. 6 GQDs and Cys-GQDs prevented the cellular seeding of mature tau fibers. Preformed tau fibrils (0.19 μM) were treated with GQDs or Cys-GQDs for 36 h, then added to cells, and incubated for an additional 48 h. Representative images of cells were taken at 20× magnification under FITC channel (ex: 469 nm/em: 525 nm). The green puncta with high fluorescence represented the aggregation of tau in cells induced by exogenous tau fibers. Scale bar: 200 μm. Tau infection (%) in the bar graph shows the number of intracellular fluorescent puncta relative to control infection wells lacking the inhibitors.

charged domains of tau, especially the aggregation-prone R2 and R3 domains, prefer to engage in more electrostatic interactions with the carboxyl groups on the edge of GQDs rather than form hydrogen bonds that are critical for the formation of tau aggregates.

Moreover, based on ThT aggregation assay results (Fig. 2c), there are other factors in addition to the negative charge of GQDs that may result in the inhibition of tau aggregation. We investigated the other potential interactions between tau and GQDs using fluorescence spectroscopy. Generally, the tau exhibits intrinsic fluorescence emission near 302 nm when excited at 265 nm, resulting from tyrosine (Tyr) fluorophores in the tau structure.[52,53] When 10 μM of tau was mixed with GQDs or Cys-GQDs in increasing concentrations, the fluorescence intensity
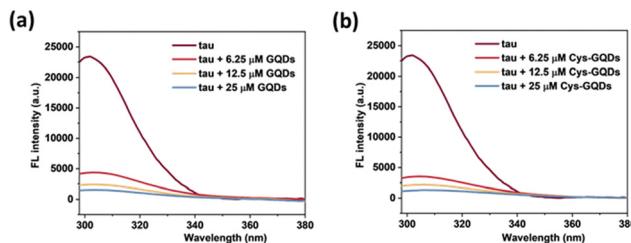
Fig. 7 Fluorescence spectra of tau protein (10 μM) incubated with 6.25, 12.5, and 25 μM of (a) GQDs and (b) Cys-GQDs (Ex: 265 nm). The fluorescence of tau was quenched significantly in the presence of GQDs or Cys-GQDs.

of tau was significantly quenched (Fig. 7), suggesting that the π-conjugated planar structure of GQDs binds with Tyr residues in tau, probably *via* π–π stacking interactions.

Besides the effect of charge, we also found that the inhibitory efficiency of GQDs increased significantly as the diameter of GQDs increased from 6.5 nm to 13.5 nm based on ThT fluorescence assay (Fig. S10, ESI†). The diameter of the full-length tau monomer is 13 ± 0.6 nm.[54] As the diameter of GQDs increases from 6.5 nm to 13.5 nm, single GQDs with a larger diameter are able to interact with more tau monomers on the edge *via* electrostatic interaction than the ones with a smaller diameter. Also, when interacting with larger GQDs, the spacing between two tau monomers increases, reducing the local concentration of tau and enhancing inhibitory efficiency. In addition, increasing the size of GQDs promotes more aromatic residues in tau to bind to the surface of GQDs *via* π–π stacking, thereby increasing the binding strength between tau and GQDs.

Overall, the potential mechanism of the interaction between GQDs and tau protein can be summarized in Fig. 8. For the aggregation of tau$_{P301L}$ (Fig. 8a), negatively charged GQDs with carboxyl groups can interact with repeat domains of tau with positive charge *via* electrostatic interactions. Meanwhile, GQDs with π-conjugated planar structure can interact with amino

acids containing aromatic rings in tau proteins *via* π–π stacking, including histidine, phenylalanine, and tyrosine. The carbon-conjugated plane of GQDs could also interact with positively charged amino acids in tau *via* cation–π interactions. For the disassembly of tau fibrils (Fig. 8b), GQDs with more negative charges can be prevented from penetrating the negatively charged fuzzy coat and accessing the fibrillar tau core, thereby reducing their efficacy in disassembly, compared to Cys-GQDs and EDA-GQDs with fewer charges. Negatively charged Cys-GQDs have a higher potential to interact with positively charged fibrillar cores compared to EDA-GQDs, which enhances their ability to disaggregate the tau fibrils.

Experimental

Materials

Sulfuric acid (95–98%) and nitric acid (69–70%) were purchased from VWR. Carbon nanofibers, *N*-hydroxysulfosuccinimide sodium salt (Sulfo-NHS, >98%), EDA (>99%), sodium acetate (>99%), ThT, heparin sodium salt, and DL-dithiothreitol (DTT, 97%) were purchased from Sigma-Aldrich. The dialysis membrane tubing (MWCO: 1kD) was purchased from Spectrum. 1-Ethyl-3-(3-dimethylaminopropyl) carbodiimide (EDC) was purchased from ThermoFisher Scientific. D-Cysteine was purchased from AmBeed. DMEM medium, Opti-MEM medium, DMEM/F12 medium, fetal bovine serum (FBS), and penicillin/streptomycin were obtained from Gibco. Cell Counting Kit-8 was purchased from Enzo Life Sciences. Lipofectamine 2000 transfection reagent was obtained from Invitrogen.

Synthesis and characterization of GQDs

GQDs were prepared using a modified Hummers' method.[35] 0.45 g of carbon fiber was added into 90 mL of concentrated H$_2$SO$_4$ (98%) and stirred for 1.5 h. After stirring, 30 mL of concentrated HNO$_3$ (68%) was added into the above mixture solution and sonicated for 1 h. Then, the mixture was reacted at 120 °C for 20 h. Next, the solution was neutralized by a sodium hydroxide solution. The final product was further dialyzed for 3 days in a dialysis bag (retained molecular weight: 1000 Da) for purification. The size and shape of GQDs were characterized by TEM (JEOL 2011). 3 μL droplet of the GQD solution (5 μM) was placed on the carbon-coated copper TEM grid (Purchased from Electron Microscopy Sciences) and allowed to dry in the air. The imaging was performed with a TEM instrument under an accelerating voltage of 200 kV. The size distribution of the GQDs was analyzed using ImageJ software. The chemical composition was performed by ATR-FTIR using Bruker Tensor 27 FTIR Spectrometer (Bruker Optics Inc., USA) with a diamond lens Attenuated Total Reflectance (ATR) module. 3 μL of 100 μM GQDs was dried in the air and each spectrum was measured as the accumulation of 64 scans at a spectral resolution of 2 cm^{-1} within the range 4000–700 cm^{-1}. The fluorescence emission property of GQDs was measured by a plate reader (Tecan infinite 200Pro). The fluorescence of GQD solution was detected at an excitation wavelength of 365 nm and an emission wavelength
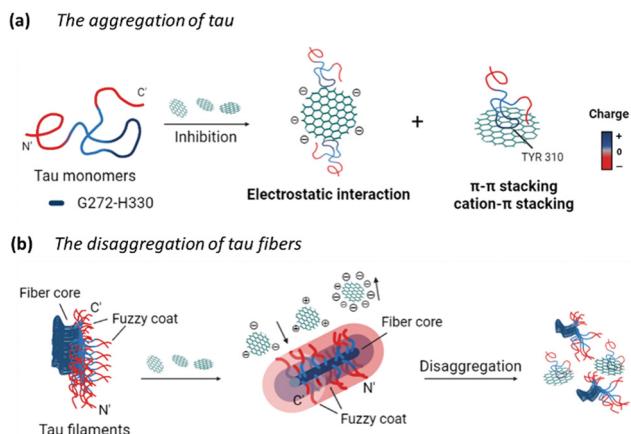

Fig. 8 Schematics of the charge effect of GQDs on their interactions with tau proteins. GQDs can interact with tau proteins *via* electrostatic interactions and π–π stacking, thereby (a) preventing the tau aggregation, and (b) inducing the disassembly of tau fibrils.

7384 | *J. Mater. Chem. B*, 2023, **11**, 7378–7388

This journal is © The Royal Society of Chemistry 2023

from 400 nm to 700 nm. The zeta potential of GQDs (6.25 μM) was calculated as the average of three test runs using Malvern Zetasizer Nano ZS (Malvern Panalytical; Worcestershire, United Kingdom). The absorption of GQDs was tested by CD spectroscopy (Jasco J-1700 Spectrometer). The GQD solution was diluted to 2.5 μM followed by spectra scanning from 200 nm to 400 nm with 0.1 nm intervals, 5 nm bandwidth, and a scan speed of 50 nm min^{-1}.

Synthesis of Cys-GQDs and EDA-GQDs

The synthesis of Cys-GQDs and EDA-GQDs was carried out using 1-ethyl-3-(3-dimethylaminopropyl) carbodiimide (EDC)/N-hydroxysuccinimide (NHS) coupling reaction.[38,55] 1 mL of EDC with a concentration of 100 mM was mixed with 25 mL GQDs (12.5 μM). After 30 min stirring, 1 mL of NHS (500 mM) was added into the mixture solution and stirred for 30 min. For Cys-GQDs, 1 mL of D-cysteine (100 mM) was added into the reaction and the mixture was reacted for 16 h. For EDA-GQDs, 0.78 mL of EDA was added into the solution and the mixture was reacted for 48 h. The product was purified by a dialysis bag with 1 K MWCO.

Tau$_{P301L}$ expression and purification

Human tau$_{P301L}$ (0N4R) with an N-terminal His$_6$ tag was purified following the previous protocol with a slight modification.[56] Briefly, transformed BL21 (DE3) cells were grown in LB + Kanamycin media at 37 °C until OD$_{600}$ reached between 0.6–0.8 and were then induced with 0.5 mM IPTG overnight at 16 °C. Cells were then harvested, resuspended, and lysed by probe sonication in the lysis buffer containing 20 mM Tris, 500 mM NaCl, 10 mM imidazole, and 5 mM serine protease inhibitor PMSF, adjusted to pH 8.0. The lysate was then boiled for 20 minutes in a water bath and the debris was pelleted by centrifugation at 20 000 g for about 40 min at 4 °C. The supernatant obtained was then injected into a 5 mL IMAC Ni-Charged affinity column and eluted over a gradient of 10–200 mM imidazole. Eluted tau-containing fractions were further purified using GE HiPrep 16/60 Sephacryl S-200 high-resolution size exclusion chromatography into a storage buffer containing 20 mM Tris, 150 mM NaCl, and 1 mM DTT, adjusted to pH 7.6. The purity of the protein was confirmed by sodium dodecyl sulfate-polyacrylamide gel electrophoresis (SDS-PAGE) analysis, and the concentration was estimated using bicinchoninic acid (BCA) assay.

ThT aggregation assay

Recombinant tau$_{P301L}$ (10 μM final concentration) and GQDs, Cys-GQDs, or EDA-GQDs (final concentration: 6.25, 3.125, 1.25, 0.625, and 0.3125 μM) were mixed in an aggregation buffer (100 mM sodium acetate, 10 μM ThT, 10 μM heparin and 2 mM DTT, pH: 7.4). 200 μL of the same solution was added into two wells of a 96-well plate for each sample. The plate was then sealed with a clear sealing film and allowed to incubate at 37 °C in a Tecan infinite 200Pro plate reader. An automated method was used to carry out ThT fluorescence measurements after 30 s shaking at an excitation wavelength of 450 nm and an emission wavelength of 485 nm at an interval of every 5 min for 45 h.

Every experiment included control wells that lacked tau$_{P301L}$, heparin, or GQDs. The aggregation curves were fitted to a Gompertz growth function according to

$$y = A e^{-e^{-k(t-t_i)}}$$

where y is defined as the normalized ThT fluorescence at time t, t_i is the inflection point corresponding to the time of maximum growth rate, A is the maximum normalized ThT fluorescence for a given sample, and k is the apparent elongation rate constant (k_{app}), in units of h^{-1}. The lag time of the aggregation curve can be calculated by $t_{lag} = t_i - \frac{1}{k}$.

IC$_{50}$ was obtained by fitting the dose-response results using a four-parameter logistic regression model, shown in the following equation.

$$y = \min + \frac{\max - \min}{1 + \left(\dfrac{x}{IC_{50}}\right)^{Hill factor}}$$

where y is defined as the endpoint normalized ThT fluorescence at concentration x, hill factor is the unitless slope factor, and max and min correspond to the maximum and minimum endpoint normalized ThT fluorescence in the range of measured concentration, respectively.

Circular dichroism spectrometry

CD spectra were measured by CD spectroscopy (Jasco J-1700 Spectrometer) at 20 °C. 10 μM of recombinant tau$_{P301L}$ and 6.25 μM of GQDs, Cys-GQDs, or EDA-GQDs were mixed in an aggregation buffer (100 mM sodium acetate, 10 μM ThT, 10 μM heparin and 2 mM DTT, pH: 7.4) and incubated for 4 days at 37 °C. Then, the tau mixture solution was diluted to 0.5 μM for measurement. Spectra were scanned from 190 nm to 260 nm, at 0.1 nm intervals, 5 nm bandwidth, and a scan speed of 50 nm min^{-1}.

Transmission electron microscopy

The preparation procedure of tau aggregation for TEM was the same as CD measurement above. A 3 μL droplet of the tau aggregation solution (10 μM) was placed on the carbon-coated copper TEM grid and wicked using filter paper after 45 s. Then, the grid was washed with 5 μL distilled water twice, and stained with 5 μL of 2% (w/v) uranyl acetate for 45 s. Grids were blotted and air-dried before imaging. A JEOL 2011 TEM was used for imaging at an accelerating voltage of 120 kV. Using ImageJ software, the lengths of amyloid fibrils were measured from the average of 16 TEM images per sample.

ThT disaggregation assay

The tau$_{P301L}$ was diluted to a final concentration of 10 μM in an aggregation buffer (100 mM sodium acetate, 10 μM heparin, 2 mM DTT, and 10 μM ThT, pH: 7.4). The protein was incubated in a microcentrifuge tube for 4 days at 37 °C. After incubation, 200 μL of the same mixture solution (5 μM tau fibers and 6.25 μM GQDs, Cys-GQDs, or EDA-GQDs) was added into two wells of a 96-well plate for each sample. The plate was then sealed with a clear sealing film and allowed to incubate at

This journal is © The Royal Society of Chemistry 2023

J. Mater. Chem. B, 2023, **11**, 7378–7388 | **7385**

37 °C in a Tecan infinite 200 Pro plate reader. An automated method was used to carry out ThT fluorescence measurements after 30 s shaking at an excitation wavelength of 450 nm and an emission wavelength of 485 nm at an interval of every 5 min for 30 h. Every experiment included control wells that lacked tau_{P301L} fibrils or GQDs.

Cellular seeding assay

HEK293 cells stably expressing tau-RD (LM)-YFP were cultured in DMEM complete medium containing 10% FBS, 1% penicillin/streptomycin, and 1% Glutamax under 5% CO_2 at 37 °C. 90 µL of cells were plated at a density of 15 000 cells per well in a 96-well tissue culture plate.

For seeding by monomeric tau, 10 µM of tau_{P301L} was incubated in an aggregation buffer containing 100 mM sodium acetate, 10 µM heparin, 2 mM DTT, and GQDs or Cys-GQDs (final concentration: 6.25 and 31.25 µM), pH: 7.4 for 4 days at 37 °C. Control vials included those in which buffer was added in place of tau_{P301L} or heparin. Following tau incubation, 8 µL of tau aggregation solution was mixed with 32 µL of low-serum Opti-MEM medium and 2 µL of Lipofectamine 2000, and the mixture solution was incubated for an additional 20 min at room temperature.

For seeding by fibrillar tau, the tau_{P301L} was diluted to a final concentration of 10 µM in an aggregation buffer containing 100 mM sodium acetate, 10 µM heparin, and 2 mM DTT, pH: 7.4. The protein was incubated for 4 days at 37 °C. Control vials included those in which buffer was added in place of tau_{P301L} or heparin. Following incubation, 8 µL of tau fibrils were mixed with 28 µL of low-serum Opti-MEM medium and 4 µL of GQDs or Cys-GQDs with different concentrations. The mixture was incubated at 37 °C for 0 or 36 h, mixed with 2 µL of Lipofectamine 2000, and incubated for 20 min at room temperature.

Then, 10 µL of mixture solution was added to HEK-293 cells and incubated for 48 h at 37 °C. Every experiment included control wells that lacked tau_{P301L}, heparin, or GQDs. After that, cells were detected by a BioTek Cytation 5 cell imager and a microplate reader. 10×10 pictures per well were taken at 20× magnification under a fluorescein isothiocyanate (FITC) channel (ex: 469 nm/em: 525 nm), and the punctate counting was carried out using built-in software.

Fluorescence quenching assay

10 µM of tau_{301L} in 100 mM sodium acetate buffer was incubated with different concentrations of GQDs or Cys-GQDs (6.25, 12.5, and 25 µM) at room temperature in a 96-well plate. After 10-min incubation, the fluorescence of the tau mixture solution was detected at an excitation wavelength of 265 nm and an emission wavelength from 295 nm to 380 nm using a Tecan infinite 200 Pro plate reader. All spectra were subtracted with GQD background solutions.

CCK-8 assay

SH-SY5Y human neuroblastoma cells were cultured in the DMEM/F12 complete medium containing 10% FBS and 1% penicillin/streptomycin under 5% CO_2 at 37 °C. 100 µL of cells

were plated at a density of 10 000 cells per well in 96-well tissue culture plates and incubated overnight. Control wells contained only medium for background measurement. Then, add 10 µL of GQDs, Cys-GQDs, or EDA-GQDs with a concentration of 15 µM and 50 µM into cells, and add 10 µL of PBS as the negative control. Incubate the 96-well microplates for 24 or 48 h in a CO_2 incubator at 37 °C. After that, change the medium, add 10 µL of Cell Counting Kit-8 reagent to cells and incubate the 96-well microplates for 3 h at 37 °C. The absorbance was measured at 450 nm using a Tecan infinite 200 Pro plate reader. The cell viability was calculated using the following equation.

$$\text{Cell viability}(\%) = \frac{A_s - A_b}{A_c - A_b} \times 100\%$$

where A_S and A_C are the absorbances measured at 450 nm for cells added GQDs and PBS, respectively, and A_b is the absorbance measured at 450 nm for only medium.

Conclusions

The aggregation of tau proteins plays a key role in the propagation of tau pathology and the observed clinical symptoms of tauopathies. However, current drug candidates for the treatment of tauopathy have shown limited success in clinical trials. Therefore, there is an urgent need for novel modulators of tau fibrillization and propagation. Here, we demonstrate that GQDs are able to prevent the seeding activity of tau fibrils by inhibiting the aggregation of monomeric tau and promoting the disassembly of tau mature fibrils. In addition, we engineered the size and charge of GQDs and investigated their interactions with tau *in vitro*. We found that larger GQDs with negative charges inhibited the aggregation of tau more efficiently, primarily *via* electrostatic and π–π stacking interactions. Our findings lay the groundwork for future investigations into the potential use of biomimetic GQDs as therapeutics for tauopathies.

Author contributions

Y. W. originated and conceptualized the study. R. Z. designed and carried out the experiments. Y. Z. developed the methodology of synthesis and functionalization of GQDs. K. M. M. and B. H. R. expressed and purified tau_{P301L}. K. M. M. developed the methodology of tau biosensor cellular seeding assay. R. Z. applied statistical and mathematical techniques to analyze data. Y. W. and J. R. D. supervised all the work. R. Z. prepared the manuscript, and all authors provided input on data interpretation, discussions, and writing.

Conflicts of interest

There are no conflicts to declare.

Acknowledgements

References

1 C. Ballatore, V. M. Y. Lee and J. Q. Trojanowski, *Nat. Rev. Neurosci.*, 2007, **8**, 663–672.

2 R. Rademakers, M. Cruts and C. van Broeckhoven, *Hum. Mutat.*, 2004, **24**, 277–295.

3 B. Falcon, W. Zhang, A. G. Murzin, G. Murshudov, H. J. Garringer, R. Vidal, R. A. Crowther, B. Ghetti, S. H. W. Scheres and M. Goedert, *Nature*, 2018, **561**, 137–140.

4 D. R. Williams, J. L. Holton, C. Strand, A. Pittman, R. de Silva, A. J. Lees and T. Revesz, *Brain*, 2007, **130**, 1566–1576.

5 P. W. Baas, A. N. Rao, A. J. Matamoros and L. Leo, *Cytoskeleton*, 2016, **73**, 442–460.

6 T. Guo, W. Noble and D. P. Hanger, *Acta Neuropathol.*, 2017, **133**, 665–704.

7 B. Nizynski, W. Dzwolak and K. Nieznanski, *Protein Sci.*, 2017, **26**, 2126–2150.

8 M. P. Mazanetz and P. M. Fischer, *Nat. Rev. Drug Discovery*, 2007, **6**, 464–479.

9 B. B. Holmes, J. L. Furman, T. E. Mahan, T. R. Yamasaki, H. Mirbaha, W. C. Eades, L. Belaygorod, N. J. Cairns, D. M. Holtzman and M. I. Diamond, *Proc. Natl. Acad. Sci. U. S. A.*, 2014, **111**, E4376–4385.

10 A. Mudher, M. Colin, S. Dujardin, M. Medina, I. Dewachter, S. M. Alavi Naini, E. M. Mandelkow, E. Mandelkow, L. Buee, M. Goedert and J. P. Brion, *Acta Neuropathol. Commun.*, 2017, **5**, 99.

11 B. Bulic, M. Pickhardt, E. M. Mandelkow and E. Mandelkow, *Neuropharmacology*, 2010, **59**, 276–289.

12 L. Wang, Bharti, R. Kumar, P. F. Pavlov and B. Winblad, *Eur. J. Med. Chem.*, 2021, **209**, 112915.

13 M. Pickhardt, Z. Gazova, M. von Bergen, I. Khlistunova, Y. Wang, A. Hascher, E. M. Mandelkow, J. Biernat and E. Mandelkow, *J. Biol. Chem.*, 2005, **280**, 3628–3635.

14 B. Bulic, M. Pickhardt, I. Khlistunova, J. Biernat, E. M. Mandelkow, E. Mandelkow and H. Waldmann, *Angew. Chem., Int. Ed.*, 2007, **46**, 9215–9219.

15 K. R. Brunden, J. Q. Trojanowski and V. M. Lee, *Nat. Rev. Drug Discovery*, 2009, **8**, 783–793.

16 K. Tatiparti, S. Sau, M. A. Rauf and A. K. Iyer, *Drug Discovery Today*, 2020, **25**, 2110–2129.

17 I. Aprahamian, F. S. Santos, B. dos Santos, L. Talib, B. S. Diniz, M. Radanovic, W. F. Gattaz and O. V. Forlenza, *J. Clin. Psychiatry*, 2014, **75**, e672–678.

18 D. M. Teleanu, C. Chircov, A. M. Grumezescu, A. Volceanov and R. I. Teleanu, *Pharmaceutics*, 2018, **10**, 269.

19 W. Zhang, N. Kandel, Y. Zhou, N. Smith, B. C. L. B. Ferreira, M. Perez, M. L. Claure, K. J. Mintz, C. Wang and R. M. Leblanc, *J. Colloid Interface Sci.*, 2022, **617**, 20–31.

20 M. Bacon, S. J. Bradley and T. Nann, *Part. Part. Syst. Charact.*, 2014, **31**, 415–428.

21 M. K. Kumawat, M. Thakur, R. B. Gurung and R. Srivastava, *Sci. Rep.*, 2017, **7**, 15858.

22 D. Iannazzo, A. Pistone, M. Salamò, S. Galvagno, R. Romeo, S. V. Giofré, C. Branca, G. Visalli and A. Di Pietro, *Int. J. Pharm.*, 2017, **518**, 185–192.

23 J. Ruan, Y. Wang, F. Li, R. Jia, G. Zhou, C. Shao, L. Zhu, M. Cui, D.-P. Yang and S. Ge, *ACS Appl. Mater. Interfaces*, 2018, **10**, 14342–14355.

24 M. C. Biswas, M. T. Islam, P. K. Nandy and M. M. Hossain, *ACS Mater. Lett.*, 2021, **3**, 889–911.

25 S. Xiao, D. Zhou, P. Luan, B. Gu, L. Feng, S. Fan, W. Liao, W. Fang, L. Yang, E. Tao, R. Guo and J. Liu, *Biomaterials*, 2016, **106**, 98–110.

26 G. Perini, V. Palmieri, G. Ciasca, M. De Spirito and M. Papi, *Int. J. Mol. Sci.*, 2020, **21**, 3712.

27 M. Suh and D. S. Lee, *Nucl. Med. Mol. Imaging*, 2018, **52**, 407–419.

28 D. Kim, J. M. Yoo, H. Hwang, J. Lee, S. H. Lee, S. P. Yun, M. J. Park, M. Lee, S. Choi, S. H. Kwon, S. Lee, S. H. Kwon, S. Kim, Y. J. Park, M. Kinoshita, Y. H. Lee, S. Shin, S. R. Paik, S. J. Lee, S. Lee, B. H. Hong and H. S. Ko, *Nat. Nanotechnol.*, 2018, **13**, 812–818.

29 Y. Yan, J. Gong, J. Chen, Z. Zeng, W. Huang, K. Pu, J. Liu and P. Chen, *Adv. Mater.*, 2019, **31**, e1808283.

30 X. T. Zheng, A. Ananthanarayanan, K. Q. Luo and P. Chen, *Small*, 2015, **11**, 1620–1636.

31 Z. B. Qu, W. J. Feng, Y. Wang, F. Romanenko and N. A. Kotov, *Angew. Chem., Int. Ed.*, 2020, **59**, 8542–8551.

32 Y. Liu, L. P. Xu, W. Dai, H. Dong, Y. Wen and X. Zhang, *Nanoscale*, 2015, **7**, 19060–19065.

33 H. Tang, Y. Li, A. Kakinen, N. Andrikopoulos, Y. Sun, E. Kwak, T. P. Davis, F. Ding and P. C. Ke, *Phys. Chem. Chem. Phys.*, 2021, **24**, 86–97.

34 Y. Wang, U. Kadiyala, Z. Qu, P. Elvati, C. Altheim, N. A. Kotov, A. Violi and J. S. VanEpps, *ACS Nano*, 2019, **13**(4), 4278–4289.

35 J. Peng, W. Gao, B. K. Gupta, Z. Liu, R. Romero-Aburto, L. Ge, L. Song, L. B. Alemany, X. Zhan, G. Gao, S. A. Vithayathil, B. A. Kaipparettu, A. A. Marti, T. Hayashi, J. J. Zhu and P. M. Ajayan, *Nano Lett.*, 2012, **12**, 844–849.

This journal is © The Royal Society of Chemistry 2023

J. Mater. Chem. B, 2023, **11**, 7378–7388 | **7387**

36 B. Geng, F. Fang, P. Li, S. Xu, D. Pan, Y. Zhang and L. Shen, *Chem. Eng. J.*, 2021, **417**, 128125.

37 L. Li, G. Wu, G. Yang, J. Peng, J. Zhao and J. J. Zhu, *Nanoscale*, 2013, **5**, 4015–4039.

38 N. Suzuki, Y. Wang, P. Elvati, Z. B. Qu, K. Kim, S. Jiang, E. Baumeister, J. Lee, B. Yeom, J. H. Bahng, J. Lee, A. Violi and N. A. Kotov, *ACS Nano*, 2016, **10**, 1744–1755.

39 J. Wang, Y. Cao, Q. Li, L. Liu and M. Dong, *Chemistry*, 2015, **21**, 9632–9637.

40 M. Zhou, Q. Shen, J. W. Shen, L. Jin, L. Zhang, Q. Sun, Q. Hu and L. Liang, *Colloids Surf., B*, 2019, **174**, 575–581.

41 M. Hutton, C. L. Lendon, P. Rizzu, M. Baker, S. Froelich, H. Houlden, S. Pickering-Brown, S. Chakraverty, A. Isaacs, A. Grover, J. Hackett, J. Adamson, S. Lincoln, D. Dickson, P. Davies, R. C. Petersen, M. Stevens, E. de Graaff, E. Wauters, J. van Baren, M. Hillebrand, M. Joosse, J. M. Kwon, P. Nowotny, L. K. Che, J. Norton, J. C. Morris, L. A. Reed, J. Trojanowski, H. Basun, L. Lannfelt, M. Neystat, S. Fahn, F. Dark, T. Tannenberg, P. R. Dodd, N. Hayward, J. B. J. Kwok, P. R. Schofield, A. Andreadis, J. Snowden, D. Craufurd, D. Neary, F. Owen, B. A. Oostra, J. Hardy, A. Goate, J. van Swieten, D. Mann, T. Lynch and P. Heutink, *Nature*, 1998, **393**, 702–705.

42 D. Chen, K. W. Drombosky, Z. Hou, L. Sari, O. M. Kashmer, B. D. Ryder, V. A. Perez, D. R. Woodard, M. M. Lin, M. I. Diamond and L. A. Joachimiak, *Nat. Commun.*, 2019, **10**, 2493.

43 C. Xue, T. Y. Lin, D. Chang and Z. Guo, *R. Soc. Open Sci.*, 2017, **4**, 160696.

44 G. Ramachandran and J. B. Udgaonkar, *J. Biol. Chem.*, 2011, **286**, 38948–38959.

45 C. L. Moore, M. H. Huang, S. A. Robbennolt, K. R. Voss, B. Combs, T. C. Gamblin and W. J. Goux, *Biochemistry*, 2011, **50**, 10876–10886.

46 M. Necula and J. Kuret, *Anal. Biochem.*, 2004, **333**, 205–215.

47 M. von Bergen, S. Barghorn, J. Biernat, E.-M. Mandelkow and E. Mandelkow, *Biochim. Biophys. Acta, Mol. Basis Dis.*, 2005, **1739**, 158–166.

48 M. Weiss, J. Fan, M. Claudel, T. Sonntag, P. Didier, C. Ronzani, L. Lebeau and F. Pons, *J. Nanobiotechnol.*, 2021, **19**, 5.

49 K. M. Makwana, M. P. Sarnowski, J. Miao, Y. S. Lin and J. R. Del Valle, *ACS Chem. Neurosci.*, 2021, **12**, 3928–3938.

50 S. Wegmann, I. D. Medalsy, E. Mandelkow and D. J. Muller, *Proc. Natl. Acad. Sci. U. S. A.*, 2013, **110**, E313–321.

51 C. Cowan and A. Mudher, *Front. Neurol.*, 2013, **4**, 114.

52 H. A. Zeinabad, A. Zarrabian, A. A. Saboury, A. M. Alizadeh and M. Falahati, *Sci. Rep.*, 2016, **6**, 26508.

53 S. Alali, G. Riazi, M. R. Ashrafi-Kooshk, S. Meknatkhah, S. Ahmadian, M. Hooshyari Ardakani and B. Hosseinkhani, *Cells*, 2021, **10**, 3521.

54 E. Mylonas, A. Hascher, P. Bernadó, M. Blackledge, E. Mandelkow and D. I. Svergun, *Biochemistry*, 2008, **47**, 10345–10353.

55 H. Park and S. Y. Park, *ACS Appl. Mater. Interfaces*, 2022, **14**, 26733–26741.

56 C. Barbereau, A. Yehya, M. Silhol, N. Cubedo, J.-M. Verdier, T. Maurice and M. Rossel, *Pharmacol. Res.*, 2020, **158**, 104865.